Supplemental Information Inventory

Figures:

Tables:

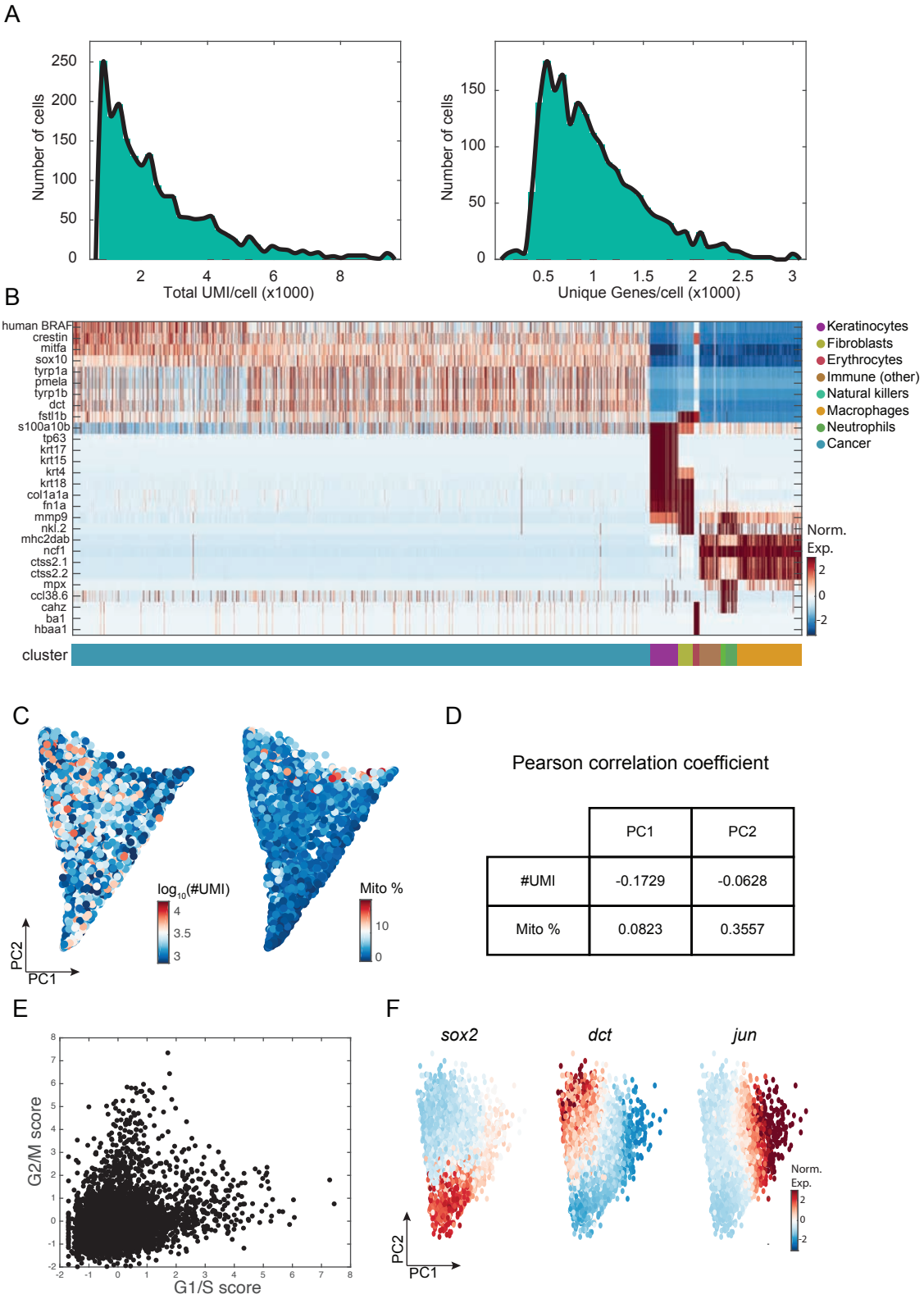

	PC1	PC2
#UMI	-0.1729	-0.0628
Mito %	0.0823	0.3557

Figure S1. Statistics and clustering on the zebrafish melanoma single-cell RNA-Seq data and PCA is not driven by technical aspects, Related to Figure 1.

(A) Histograms of the number of UMIs (left) and genes (right) detected per cell.

(B) Heatmap of all tumor cells clustered by hierarchical clustering (see Methods), showing gene expression levels for the selected marker genes across the cell type population (Table S1). The bottom bar indicates the assigned cell type identity corresponding to Figure 1b.

(C) PCA of the cancer cells (as in Figure 1) colored by the total number of UMIs detected (left) and the fraction of the transcriptome that is accounted for by mitochondrial genes (right).

(D) Table describing Pearson correlation coefficients with PC1 and PC2 scores.

(E) Cell cycle state inferred from single-cell RNA-Seq. The x- and y- axes indicate the average expression of G1/S and G2/M genes, respectively.

(F) PCA of the malignant cells without smoothing pre-processing. Cells are colored by the smoothed expression of genes marking each of the three transcriptional programs to indicate their persistence: sox2, neural crest; dct, mature melanocyte; jun, stress-like.

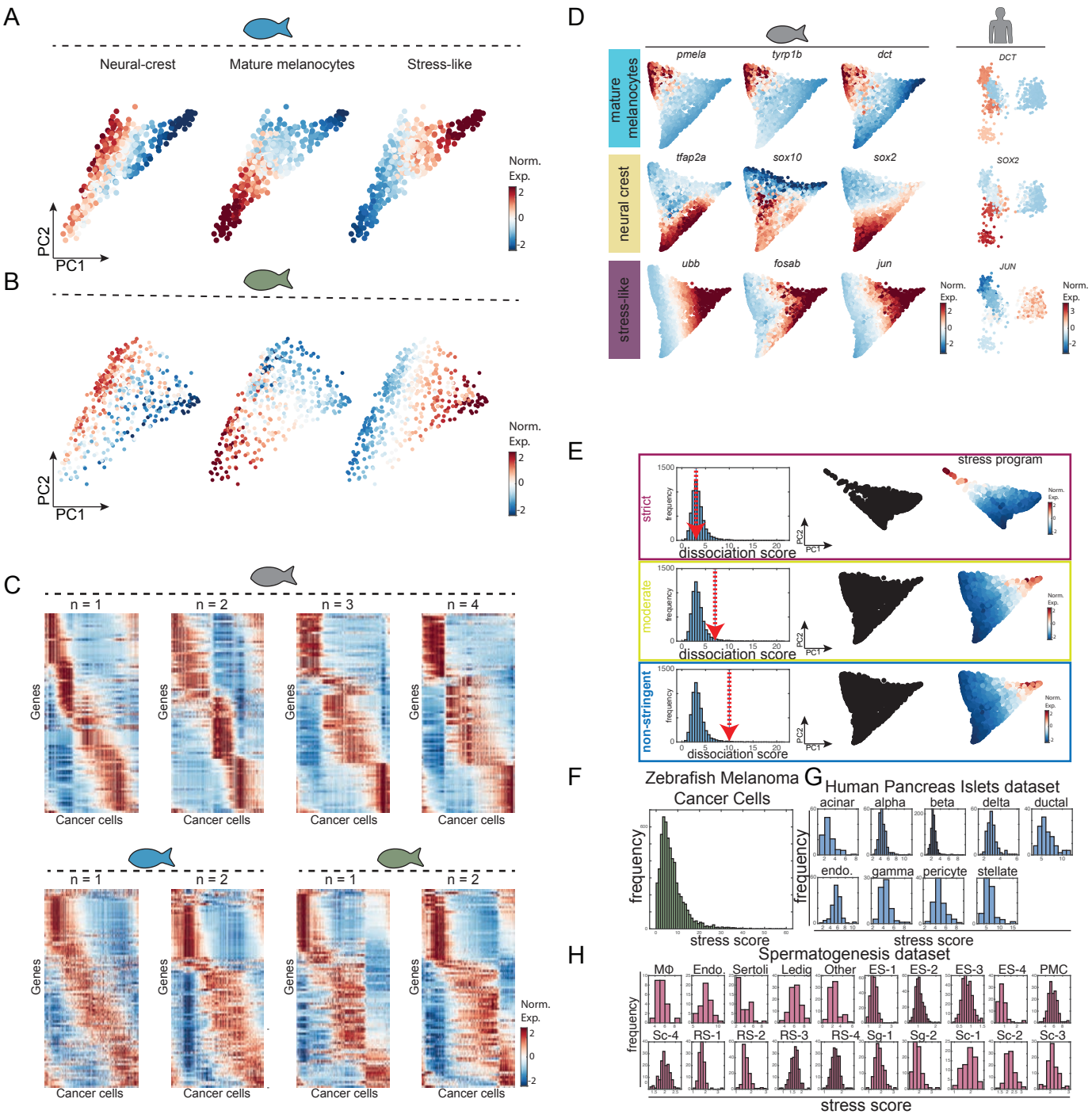

Figure S2. The stress-like cancer cell state is robust and not an artifact of the cell dissociation protocol, Related to Figure 2.
(A,B) Gene expression levels for the neural crest, mature melanocyte, and stress-like programs, mapped onto PC1 and PC2 on the tumor cancer cells for each biological replicate.
(C) Heatmaps showing the expression of all genes defining the neural crest, mature melanocytes and stress-like transcriptional program, for each tumor and its multiple biopsies.
(D) Gene expression levels for the indicated genes, mapped onto the PCA-space shown in Figure 1c (left three columns). The fourth column shows the expression of the indicated human genes in a PCA computed using previously reported human single-cell RNA-Seq data (Tirosh et al., 2016a).
(E) *In silico* purification based on the van den Brink et al. method. Left - Distribution of dissociation scores across all cancer cells with strict (top), moderate (middle) and non-stringent (bottom) thresholds. Middle – PCA on the remaining cancer cells after removing all cells that do not meet the dissociation score threshold. Right – The PCA plot with cells colored by the expression level of the stress-like program.
(F) Distribution of stress-like program scores, defined as the sum of expression of all genes of this program divided by the expression of all genes in a given cell, across all cancer cells.
(G,H) Same as (F) for human islets (Baron et al., 2016) and spermatogenesis (Xia et al., 2020) datasets, separated according to cell types.

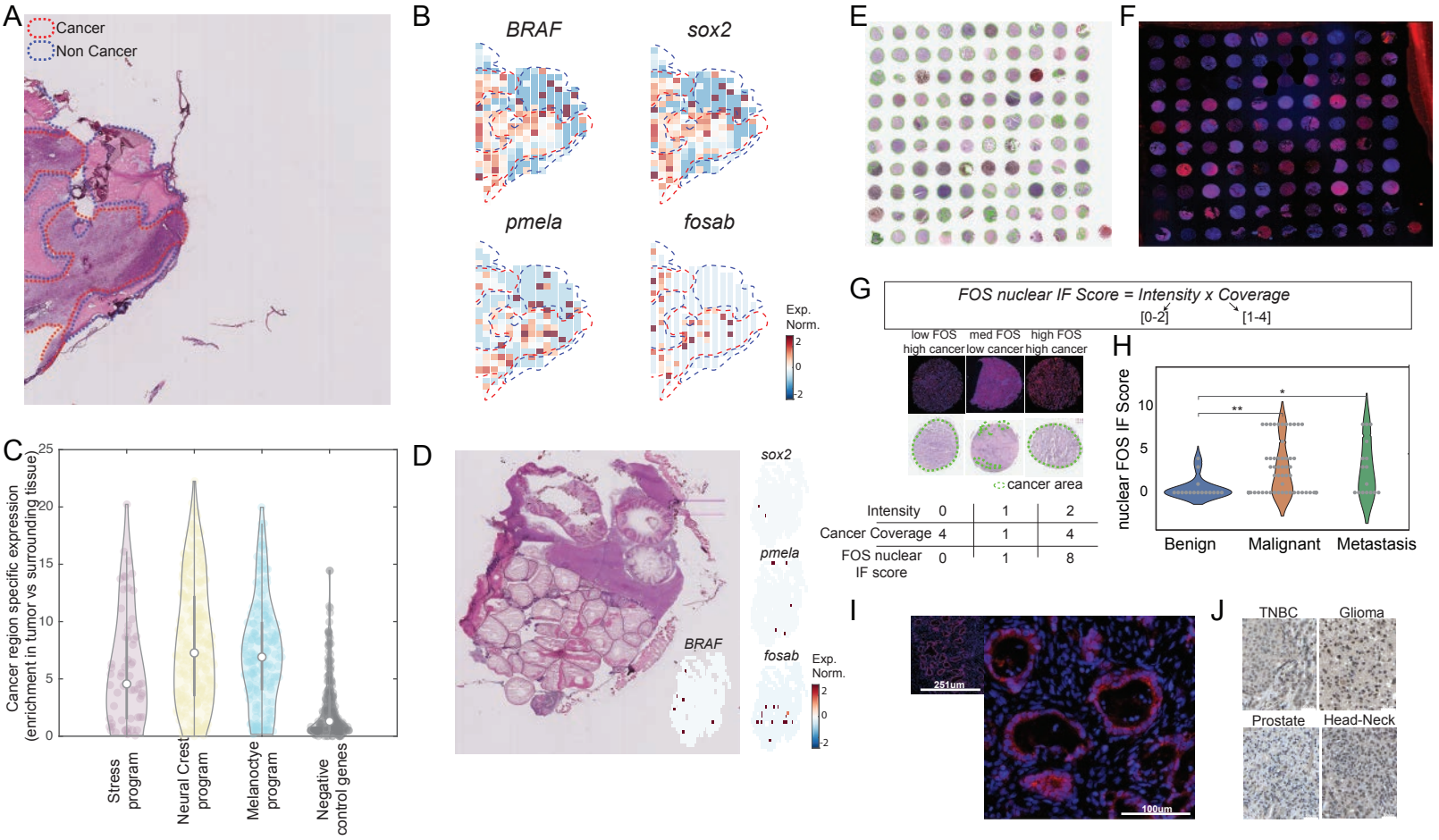

Figure S3. Spatial transcriptomics analysis, immunofluorescence and protein expression of the stress-like state maker FOS protein in human sections, Related to Figure 3.

(A) Hematoxylin and eosin stain of a zebrafish transplanted tumor section. Red and blue dotted lines mark cancer and non cancer areas, respectively.

(B) Gene expression profiles of the indicated genes obtained by spatial transcriptomics performed on a section adjacent to the one shown in panel A. human $BRAF^{V600E}$ transgene is a marker for the cancer region; sox2 is a marker for the neural crest state; pmela is a marker for the mature melanocyte state; and fosab is a marker for the stress-like state.

(C) Violin plots indicating the enrichment of each gene (Man-Whitney test, $-\log_{10}$ of the P-value) in each of the indicated programs. The negative control represents a randomly selected set of 200 genes.

(D) Hematoxylin and eosin stain of a non-tumor zebrafish section and gene expression profiles of the indicated genes obtained by spatial transcriptomics performed on an adjacent section.

(E) Hematoxylin and eosin staining of a tumor microarray containing 100 human melanoma cores (Biomax, ME1004g). Green lines indicate cancer areas.

(F) FOS immunofluorescence (red) and DAPI (blue) staining performed on the tumor microarray shown in (E).

(G) FOS immunofluorescence scoring methodology. To quantify the range and intensity of FOS staining, we computed the product of the staining intensity (0-2 scale) and coverage of cancer cells (1-4 scale), yielding an index ranging from 0 to 8. Below the immunofluorescence score, definition examples for low, medium and high FOS IF intensities are shown (see Methods).

(H) Violin plots of nuclear IF score distributions across 100 tumor microarray core sections. Shown are the distribution of FOS IF scores across the sections, indicating that malignant and metastatic sections showed higher FOS scores when compared to the benign sections; $P<10^{-4}$ and $P<10^{-2}$, respectively.

(I) FOS immunofluorescence (red) on pancreatic ductal adenocarcinoma (PDAC) section with DAPI nuclear staining (blue).

(J) FOS immunohistochemistry images from the human protein atlas (Thul et al., 2017; Uhlén et al., 2015) for breast, glioma, prostate, and head-neck adenocarcinoma cancers.

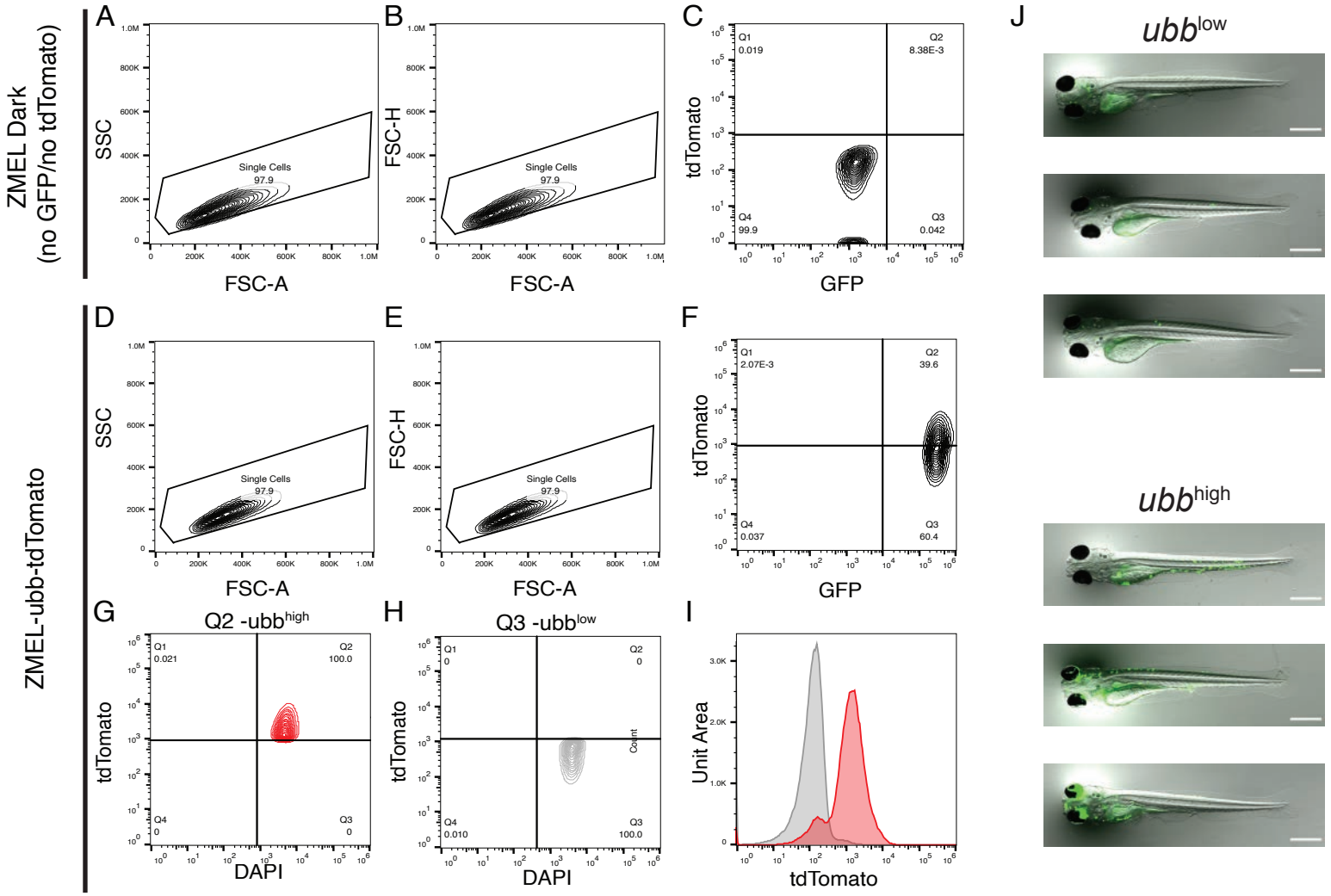

Figure S4. FACS analysis of ZMEL-ubb-tdTomato cells, related to Figure 4.
(A) Forward scatter vs side scatter of ZMEL cells with no GFP or tdTomato for the selection of live cells.
(B) forward scatter area vs height of the cells gated in (A) for the selection of single cells.
(C) GFP vs tdTomato intensities in logarithmic scale for cells gated in (B) to define populations.
(D-F) same as A,B,C but for ZMEL-ubb-tdTomato cell line, respectively.
(G) tdTomato intestinsity vs DAPI of the ubb^{high} population defined by the gate Q2 in F.
(H) tdTomato intestinsity vs DAPI of the ubb^{low} population defined by the gate Q3 in F.
(I) histograms of the populations in G and H after 6 weeks of the original sorting.
(J) Additional images of zebrafish embryos injected with ZMEL1-GFP;ubb-tdTomato cells. Cells sorted to low and high levels of tdTomato in panel (I) injected into zebrafish for tumor initiation assay followed by quantification of GFP intensity.

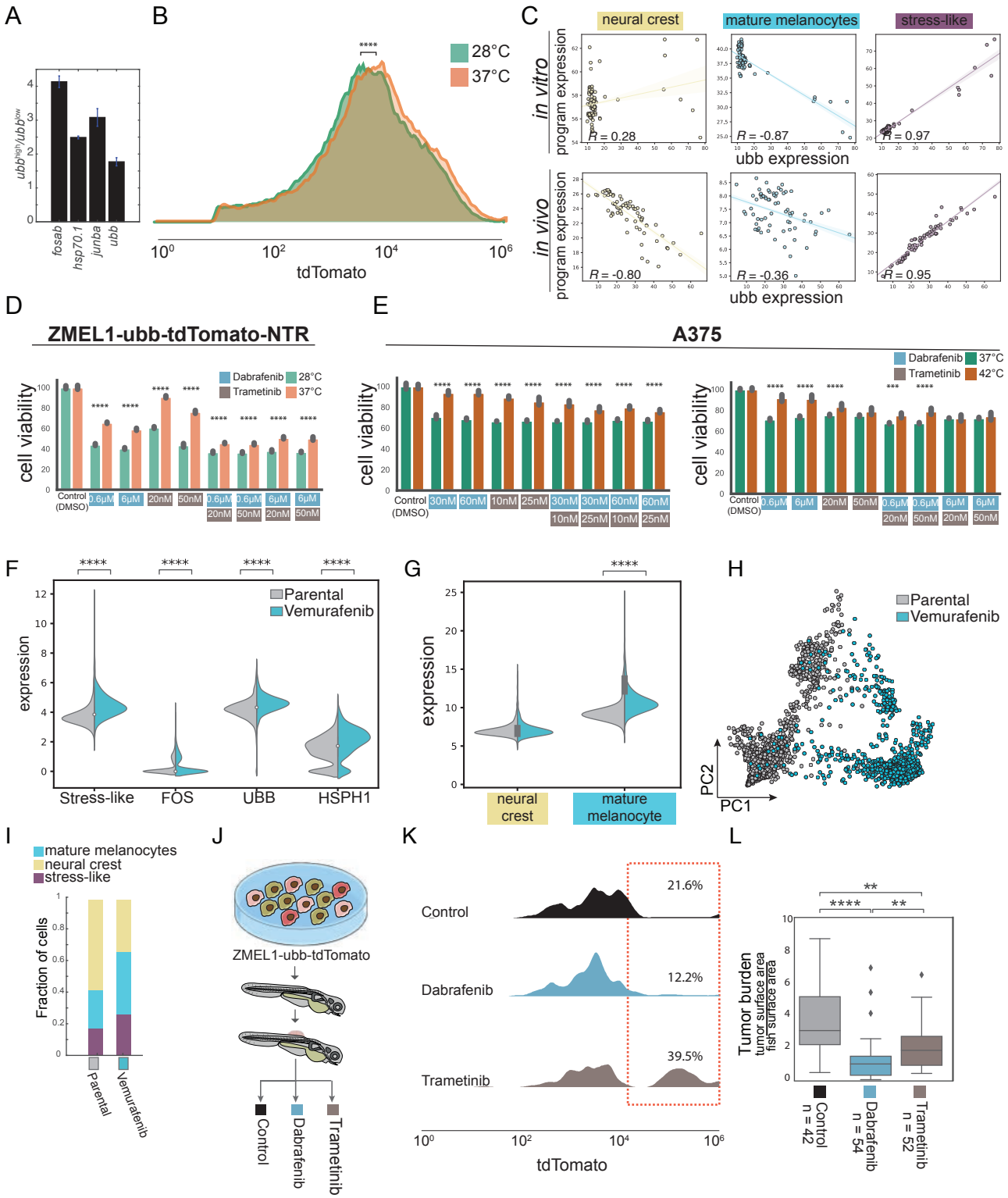

Figure S5.The stress-like state is associated with drug resistance, related to Figure 4.

(A) Bar plot describing the fold change in expression of the indicated genes related to the stress-like program, when comparing ubb^{high} cells to ubb^{low} cells measured by qPCR.

(B) Distributions of tdTomato intensities of 100,000 events recorded under optimal growth (green) and heat-shock (orange) conditions.

(C) Scatter plots of ubb expression vs the entire neural crest program (left), mature melanocyte program (middle) and the stress-like program (right) in ZMEL1-GFP single cells in vitro (top) and in vivo (bottom).

(D,E) ZMEL1-ubb-tdTomato-NTR and A375 cell viability assays under heat shock and drug treatment, respectively. Bar plots representing cell viability across culturing conditions (optimal/heat shock).

(F,G) Violin plots for the stress-like gene program and representative genes, the neural-crest and mature melanocytes gene programs, respectively, before and after treatment with vermurafenib, a BRAF inhibitor (Ho et al., 2018) (Mann-Whitney test, ****, P<10-4).

(H) PCA projection of the same cells as in (F,G). Coefficients were taken from Figure 3E. Color indicates treatment group.

(I) stacked bar plot indicating the proportions of the transcriptional cell states detected before and after treatment with BRAF inhibitor.

(J) Experimental schematic for testing if the stress-like state is associated with drug resistance *in vivo.*

(K) FACS histograms quantifing the number of ubb^{high} versus ubb^{low} cells based on tdTomato intensity.

(L) Boxplots indicating tumor burden quantified by GFP intensity of the three different treatment groups (Mann-Whitney test; ****, P<10^{-4}; **, P<10^{-2}, respectively).

Table S1. Cell type marker genes, Related to Figure 1.

Cell type	Genes
Cancer	*hBRAF, crestin, sox10, mitfa, tyrp1a, tyrp1b, dct, pmela (Kaufman et al., 2016)*
Keratinocytes	*tp63, krt4 (Eisenhoffer et al., 2017)*
Fibroblasts	*fn1a, col1a1a, fstl1b, s100a10b (Gistelinck et al., 2016; Maruyama et al., 2016)*
Erythrocytes	*ba1, hbaa1 (Kulkeaw and Sugiyama, 2012)*
Natural Killers	*nkl.2, ccl38.6 (Carmona et al., 2017)*
Neutrophils	*mpx, mmp9, ncf1 (Carmona et al., 2017)*
Macrophages	*ctss2.1, ctss2,2, mhc2dab (Carmona et al., 2017)*

Table S2. Transcriptional programs of the identified cancer cell states, Related to Figure 2.

Mature melanocytes		Neural crest			Stress-like
ACTB	HNRNPA0	ABCF1	HSPA9	SMAP1	AHSA1
ACTR1B	HNRNPD	ABI2	HSPB1	SNCG	ATF3
ALDH7A1	HSPE1	ACSL4	IFI27	SNRPB	B2M
ALDH9A1	IFI44	ACTN1	IFI27L1	SNRPD1	BRD2
ANP32A	KARS	ACVRL1	IFI27L2	SOX10	BTG1
ANXA1	KMT5A	ADCYAP1	ILF2	SOX2	BTG2
ANXA2	KRT8	ADD3	ITGA5	SPIRE1	CCER1
ANXA4	LDHB	AK2	ITM2B	SPRY4	CCNG1
ANXA5	LMNB1	AKAP8L	JAK1	SSB	CHCHD2
AP2M1	LMNB2	ALCAM	JAM3	ST8SIA6	CIRBP
AQP3	LOXL2	AP1B1	KPNB1	STAT2	CYR61
ARPC3	LSM7	APLP2	LGMN	SUMO1	DNAJB1
ARPC5	MARCKSL1	ARL6IP1	LYPLA2	SYT11	DUSP1
ARRDC3	MDH1	ATAD2B	METAP1	TBC1D10A	DUSP2
ATP5B	MDH2	ATF4	MITF	TCN2	DUSP5
ATP5C1	MIF	ATP1B1	MLPH	TFAP2A	EGR1
ATP5D	MTPN	ATP1B3	MOV10	TFAP2C	EGR2
ATP5F1	MYH7B	ATP5A1	MPEG1	TFAP2E	FOS
ATP5G1	MYL12A	ATP5E	MT2A	TFRC	FOSB
ATP5O	MYL6	ATP5G3	MTMR6	TMC5	FOSL1
ATP6V0E1	NDUFA1	BCKDK	MYCBP	TMEM30A	GADD45B
BLOC1S6	NDUFA8	BLCAP	MYCN	TMEM50A	HES1
BTG3	NPM1	BTF3	MYO5B	TMEM59L	HES4
C15orf48	PABPC1	C6orf62	NACA	TP53I11	HIST2H2AB
C21orf33	PAH	CALM3	NCL	TPT1	HSP90AA1
CALM1	PAICS	CAPN2	NDRG1	TXNIP	HSPA1L
CALML3	PALM	CAPZA1	NDUFA4	U2AF2	HSPA4
CAPG	PBDC1	CAV1	NDUFS5	UQCRC1	HSPA5
CAPZB	PCBD1	CCND1	NME1	VCP	HSPA8
CCDC80	PFN1	CCNI	NMRK2	VPS26A	HSPH1
CCT3	PFN2	CDH1	NPEPL1	WBP2NL	ID2
CCT8	PKM	CDK15	NSA2	YWHAB	ID3
CD81	PLPP1	CDKN1B	NTNG2	YWHAG	IER2

CDC42SE1	PMEL	CEP170	NTRK3	ZBTB20	IER5
CFL1	POMP	CFH	NUDC		JDP2
CIRBP	POR	CHUK	OAZ1		JUN
CKAP2	PPIA	CIART	OLA1		JUNB
CKB	PPIB	CLIC4	PA2G4		JUND
CLU	PPP2CB	CNTFR	PABPC1		MCL1
CNBP	PRDX1	COL9A2	PABPN1		MIDN
COBLL1	PRDX2	COX6C	PDCD6IP		MKNK2
COPB2	PRDX6	CSNK2A1	PDLIM1		NFKBIA
COPE	PSMA2	CSNK2B	PEF1		NR4A1
COPS4	PSMA3	CSTB	PFDN5		NR4A3
COX4I2	PSMB6	CTSH	PGAM1		PDCD4
COX6B1	PSMC3	CTSL	PGK1		PLK3
COX7A2	PSMC5	CTSZ	PIK3CA		PNRC2
CSRP2	PSME2	CXXC5	PLA2G7		PPP1R15A
CSTB	PSMG1	CYC1	PLEC		RHBDD1
CTSL	PTGR1	CYCS	PNO1		RSRP1
DAD1	QDPR	DCBLD1	PNOC		SGK1
DAP	RAD21	DDX21	PPP1R1B		SKIL
DAPL1	RAN	DUSP6	PRMT1		SLC38A2
DBI	RAP1B	EDNRA	PSAP		SOX4
DCT	REEP5	EEF1A2	PSMB1		SQSTM1
DDC	RHOC	EEF1B2	PTP4A2		STIP1
DDOST	RPN1	EEF1D	PTPRE		TOB1
DENR	RTN1	EIF2S2	PVALB		UBB
DYNC1LI2	S100A10	EIF2S3	QKI		UBC
EEF1G	S100A4	EIF3G	RAB5A		WSB1
EEF2	SEC13	EIF3I	RABL6		ZFAND2B
EFEMP2	SEC61B	EIF4B	RACK1		
EHD1	SELENOF	EIF4EBP2	RDH8		
EIF4A1	SLC25A5	EIF5	RGL1		
EIF5A2	SLC39A10	EIF5A	RGS12		
ELOVL1	SOD1	EMILIN1	RHPN2		
ENO1	SPON2	EMP3	RNASET2		
ETF1	SSR4	ENPP1	ROMO1		
FHL1	SUB1	FABP3	RPL22L1		
FNDC5	SYNGR3	FAM107B	RPLP2		

FSTL1	TCP1	FAM126A	RPS26		
FXYD6-FXYD2	TFG	FAU	RSL24D1		
GAPDHS	TIMP2	FGFR4	RTN4		
GDI1	TKTL2	FNBP1L	RUNX3		
GLRX	TMA7	GADD45A	SASH1		
GM2A	TMED2	GLO1	SDC4		
GPR143	TMEM163	GLUL	SDHA		
GPX3	TTR	GNB1	SDPR		
GPX4	TUBB4B	GNG2	SEH1L		
GSTP1	TYRP1	GNG3	Sep9		
GSTT1	UBE2L3	GNPDA2	SERBP1		
GYG1	UFM1	GPI	SF3A3		
H2AFZ	UQCRC2	H1FX	SGPL1		
HIGD1A	VIM	H2AFY2	SH3BGRL3		
HINT1	YWHAB	HDAC1	SH3GLB1		
HM13	YWHAE	HDLBP	SHFM1		
HMGA1	YWHAQ	HNRNPAB	SLC20A1		
HMGB2		HNRNPR	SLC25A22		
HMGN2		HPS1	SLC2A11		